Convective and orographic origins of the mesoscale kinetic energy spectrum

Salah Kouhen [1], Benjamin A. Storer [2], Hussein Aluie [2,3,4], David P. Marshall [1], Hannah M. Christensen [1]

[1]Department of Physics, University of Oxford, Oxford, United Kingdom
[2]Department of Mechanical Engineering, University of Rochester, Rochester, NY, USA
[3]Department of Mathematics, University of Rochester, Rochester, NY, USA
[4]Laboratory for Laser Energetics, University of Rochester, Rochester, NY, USA

Key Points:

- Global maps of spectral slope are produced through a novel coarse-graining method
- Orography and precipitation shallow the spectral slope in the troposphere significantly
- Conditioned spectra quantify the relationship between slope, orography, precipitation and energy flux

---

Corresponding author: Salah Kouhen, `salah.kouhen@physics.ox.ac.uk`

Abstract

The mesoscale spectrum describes the distribution of kinetic energy in the Earth's atmosphere between length scales of 10 and 400 km. Since the first observations, the origins of this spectrum have been controversial. At synoptic scales, the spectrum follows a –3 spectral slope, consistent with two-dimensional turbulence theory, but a shallower –5/3 slope was observed at the shorter mesoscales. The cause of the shallower slope remains obscure, illustrating our lack of understanding. Through a novel coarse-graining methodology, we are able to present a spatio-temporal climatology of the spectral slope. We find convection and orography have a shallowing effect and can quantify this using "conditioned spectra". These are typical spectra for a meteorological condition, obtained by aggregating spectra where the condition holds. This allows the investigation of new relationships, such as that between energy flux and spectral slope. Potential future applications of our methodology include predictability research and model validation.

Plain Language Summary

The kinetic energy spectrum describes how much energy is at different spatial scales in the atmosphere, from km-scale atmospheric waves to large-scale weather systems 1000 km across. This distribution may influence predictability. Edward Lorenz argued that the spectrum can determine whether a fluid can be forecast arbitrarily far into the future or not. In this paper, we employ a novel method to reveal how the spectrum varies in different locations on Earth. In addition, we generate the first "conditioned spectra", which are the aggregated spectra for different levels of orography, convection and energy transfer. We are able to demonstrate the tendency of convection and orography to increase small-scale energy and show their effect on the classic global spectrum. Spectra are vital for model validation and predictability research; therefore, these results and the methods used to obtain them are of interest to meteorology practitioners, theorists and those in neighbouring fields.

1 Introduction

The reader familiar with turbulence theory may recognise $-5/3$ as the spectral slope of three-dimensional turbulence, which arises from a cascade of energy from large to small scales (Kolmogorov, 1941). However, the aspect ratio, stratification and rotation of the atmosphere all conspire against this explanation for the atmospheric mesoscale slope (G. K. Vallis, 2017). Similarly, two-dimensional turbulence exhibits a –5/3 slope at scales larger than an injection of energy. The latter result motivated early explanations for the shallowing as being caused by small - submesoscale - energy injection from convection (Gage, 1979; Lilly, 1983; G. Vallis et al., 1997), but this explanation became less popular once the average flux of energy was discovered to be towards the smaller scales in the mesoscales (Lindborg, 1999; Cho & Lindborg, 2001; Lindborg & Cho, 2001; Augier & Lindborg, 2013). Other turbulence-based explanations include the two-dimensional surface quasi-geostrophic equations which exhibit a direct, down-scale cascade with a $-5/3$ law (Tulloch & Smith, 2009). However, the validity of these equations to explain the global shallowing is called into question by their assumption of geostrophic balance (Callies et al., 2014).

Explanations that move away from the concept of a turbulent inertial range have gained prominence, such as wave theories and convective and orographic theories (Dewan, 1979; Waite & Snyder, 2009; Sun et al., 2017), while competing explanations such as stratified turbulence have also been put forward (Lindborg, 2006; Waite & Bartello, 2006). More recently, a mix of explanations has been posited, and the inability of a single theory to explain the spectral shallowing has been suggested (Selz et al., 2019; Aaron Wang & Sardeshmukh, 2021), but no consensus has yet been reached.

To address this problem as well as explore the spatial dependence of spectral slope, we employ sequential coarse-graining to extract instantaneous spatial maps of kinetic energy (KE) at multiple scales, allowing the creation of local power spectra (Sadek & Aluie, 2018; Storer & Aluie, 2023). These spectra can be conditioned based on geography and meteorology, creating 'typical' spectra for the conditions, or they can be combined to measure the full global spectrum as would be found through a Fourier or spherical harmonic method (Storer et al., 2022; Buzzicotti et al., 2023). We can investigate the slope of the power spectra at different locations and under different meteorological conditions, allowing us to analyse a vast range of geophysical data and atmospheric phenomena in a novel way.

Methods

Coarse-Graining

A commutative coarse-graining method, implemented in FlowSieve (Storer & Aluie, 2023), is applied to atmospheric data. This analysis framework has been used to study global KE spectra of the ocean (Storer et al., 2022; Buzzicotti et al., 2023) as well as the across-scale oceanic KE transfer (Storer et al., 2023). At its core, coarse-graining uses spatial filtering — convolution with a filtering kernel — to partition both scalar and vector fields into small-scale and large-scale components, where the partition scale is arbitrarily set. This filtering procedure can be applied to both types of datasets as well as the governing equations / physics, allowing us to study and quantify the scale-dependence of the physical system (Aluie et al., 2018). Importantly, when applied in a careful way, coarse-graining commutes with spatial derivatives, ensuring preservation of key flow properties like incompressibility (Aluie, 2019).

Details of the commutative coarse-graining methodology are outlined in those papers (Storer et al., 2022; Buzzicotti et al., 2023; Storer et al., 2023; Aluie et al., 2018; Aluie, 2019), and here we instead provide details of the novel developments on that framework, namely the extension to local spectral slopes. For a given filter scale ℓ, coarse-graining provides large-scale KE as a function of space, time, and scale: $\mathrm{KE}^{>\ell}(\vec{x},t)$. Following (Sadek & Aluie, 2018), the KE spectral density is then given by $\frac{\partial}{\partial k}\mathrm{KE}^{>\ell}(\vec{x},t)$, where $k=\ell^{-1}$, which remains a function of space, time, and scale. Since power laws of the form k^{α} become straight lines under a log-log transformation, spectral slope is generally defined as the log-log slope of the power spectrum. Specifically, given a scale- and space-local KE, the spectral slope can be defined as

$$\text{Spectral Slope} = \frac{\partial}{\partial \log k}\left(\log\left[\frac{\partial}{\partial k}\mathrm{KE}^{>\ell}\right]\right)(\vec{x},t,\ell) \tag{1}$$

$$= k\,\frac{\frac{\partial^2}{\partial k^2}\mathrm{KE}^{>\ell}}{\frac{\partial}{\partial k}\mathrm{KE}^{>\ell}}. \tag{2}$$

This definition provides a scale- and space-local measurement of the spectral slope.

Filtering Kernel

For a given scalar field f on the sphere Ω and filtering scale ℓ, the coarse-grained form of f, denoted $\overline{f}$, is defined as

$$\overline{f}(\vec{x},t) = \int_{\vec{y}\in\Omega} f(\vec{y},t)G(\gamma(\vec{x},\vec{y}))dA, \tag{3}$$

where $\gamma(\vec{x},\vec{y})$ is the geodesic distance on the sphere and G is the filtering kernel. In this work we define the kernel by

$$G(\delta) = \frac{1}{A}\left[\frac{1}{2}\left(1-\tanh\left(10D(\delta)\right)\right) - c\cdot\exp\left(-\left(2D(\delta)\right)^2\right)\right], \tag{4}$$

where A, c are normalization factors and $D(\delta) = {}^{\delta}/_{(\ell/2)} - 1$.

Practical Details of Spectral Slopes

It is worth noting that some care needs to be taken when computing statistics of the spectral slope. Since spectral slopes are only concerned with the log-log slope, two spectra that differ by a constant scaling factor (i.e. $\mathrm{KE}_1^{>\ell} = \alpha\cdot\mathrm{KE}_2^{>\ell}$) have the same slope. That is, spectral slope is insensitive to KE magnitude. Because of this, it is dynamically inconsistent to, for example, compute means of the slopes directly. To illustrate, consider two spectra, one with very high energy and a -3 slope, and the other with very low energy and a -2 slope. Because of the energy disparity, the average of the spectra would essentially follow the high-energy -3 curve, giving an average slope of ~ -3, while computing the mean of the slopes themselves would give -2.5. Following the definition of equation 2, we can see that the problem is because averaging does not commute with the ratio. Instead, we compute the weighted mean, using the KE spectrum (the denominator in eq. 2) as the weight. In other words, the mean of the spectral slopes should be measured as the slope of the mean power spectrum, not a direct mean on the slopes themselves. This is discussed further in the Supporting Information.

Noisy Slopes

It is also worth recognizing that clean power law signals typically only exist in aggregate, and not at a single instance in time and space. As a reflection of this, spectral slopes computed at a single time and length scale will typically produce a noisy signal. Taking means over larger spatial areas [e.g. coarsening to $2^\circ\times2^\circ$ resolution], time means [e.g. monthly, seasonal, etc], and averaging across a scale band [e.g. between 100 km and 400 km] provide meaningful ways to remove spurious slopes caused by low-energy signals.

In Figure 1, time-averaging, averaging onto a $2^\circ \times 2^\circ$ grid, and averaging across scales between 100 and 400 km are used to reduce the noise. Figures 2 and 3 used a combination of temporal averaging (inherited from the time-space binning used for conditioning) as well as averaging over the mesoscales [between 100 km and 400 km] for the slopes reported in the legends.

Comparison with Alternative Methods

It is important to note that other methods for studying spectral characteristics are typically unable to build spatial maps. For example, (Buzzicotti et al., 2023) illustrates how using spherical harmonics to create spatial maps of coarse KE produces heavy spectral ringing and truncation artefacts, which can dominate in low-energy regions. Recently, (Aaron Wang & Sardeshmukh, 2021) used truncated spherical harmonics to produce spatial maps of KE within different scale bands, as well as of spectral slopes. While this is a pragmatic solution to the problem, there are concerns with their framework that are overcome by coarse-graining. The first is that of spectral ringing: as highlighted by (Buzzicotti et al., 2023) and analogous to Fourier methods, truncating spherical harmonics produces spectral ringing artefacts, which are most visible in (Aaron Wang & Sardeshmukh, 2021) Figure 3(a)-(c). Further, their definition of spectral slope [unnumbered equation on their page 2595] assumes that the scale range being measured presents a single consistent power law, which need not be true a priori. Coarse-graining naturally produces spatial maps that guarantee that information is space-local to within a radius of $\ell/2$, in contrast to the inherently global nature of spherical harmonics. Further, since spectral slopes in commutative coarse-graining only require first and second derivatives of the large-scale KE, the slopes can be measured as a function of length-scale, and do not require any prior assumptions about the slope other than that they are shallower than the critical slope.

Difference in Energy Formulation vs Spherical Harmonics It is important to emphasise that spherical harmonics (and Fourier methods in general), while globally energy-preserving through Parseval's relation, are not locally energy-preserving decompositions. That is, $|u^{<K}|^2+|u^{>K}|^2 = |u|^2$ need not hold locally under a spherical harmonic framework. While coarse-graining can use a Dirichlet kernel to perform a spherical harmonic decomposition, our definition for energy within a wave-band, being an ℓ^{-1}-derivative of the *space-local* coarse/fine KE, is fundamentally different. This difference then extends to our definition for spectral slope, which uses first and second ℓ^{-1}-derivatives of the space-local coarse KE. Our approach then departs not only in our choice of filtering kernel, but early in the formulation of local energy, from a traditional spherical harmonics approach.

Dataset

The European Centre for Medium-range Weather Forecasting (ECMWF), integrated forecasting system operational analysis provides a high-resolution ($^1/_{12}{}^\circ$) dataset that assimilates observational data. This dataset provides a physically and observationally constrained best estimate of the instantaneous state of the global atmosphere. In contrast to ERA5, which shows no distinct mesoscale shallowing due to resolution and other issues, the ECMWF operational analysis demonstrates a clear shallowing that agrees well with high-resolution global simulations (Aaron Wang & Sardeshmukh, 2021; Stephan et al., 2022). We analysed the whole of 2020, with hourly means sampled 4 times per day 00, 06, 12, 18 UTC, at both 200 and 600 hPa pressure levels. Precipitation and orography data were sourced from ECWMF ERA5 for 2020 (Hersbach et al., 2020).

Domain Partitioning: Category definitions and sample sizes

The sample size and category details are given in Supporting Information. To obtain confidence bounds bootstrapping was employed. For each spectrum examined, traditional bootstrapping was employed with 256 samples. A parameter sweep was employed to ensure statistics had sufficiently converged for this number of samples.

Results and Discussion

Figure 1 shows the global distribution of the mesoscale spectral slope that we compute using a high-resolution global atmosphere dataset for 2020, a mixed-phase El Niño year. The 200 hPa level (Figure 1d), at around 12 km altitude, straddles the troposphere and the stratosphere, while 600 hPa (Figure 1a), corresponding to 4 km altitude, is within the troposphere.

The KE spectral slopes at those pressure levels demonstrate striking spatial patterns. The inter-tropical convergence zone (ITCZ) paints a slash across the oceans, clearly demonstrating a high correlation with precipitation, which indicates convective activity. The South Pacific convergence zone and storm tracks are also visible. Orography also clearly shows a shallowing effect at 600 hPa over the Rockies, the Andes, the Atlas mountains and East African highlands, the Urals and the Himalayas (see annotations in 1b). The shallowing effect of orography attenuates with altitude but can still be discerned at 200 hPa, for instance, over the Rockies and Southern Andes. These observations broadly match those presented in the lower resolution analysis in (Aaron Wang & Sardeshmukh, 2021). See methods for a comparison of our approaches.

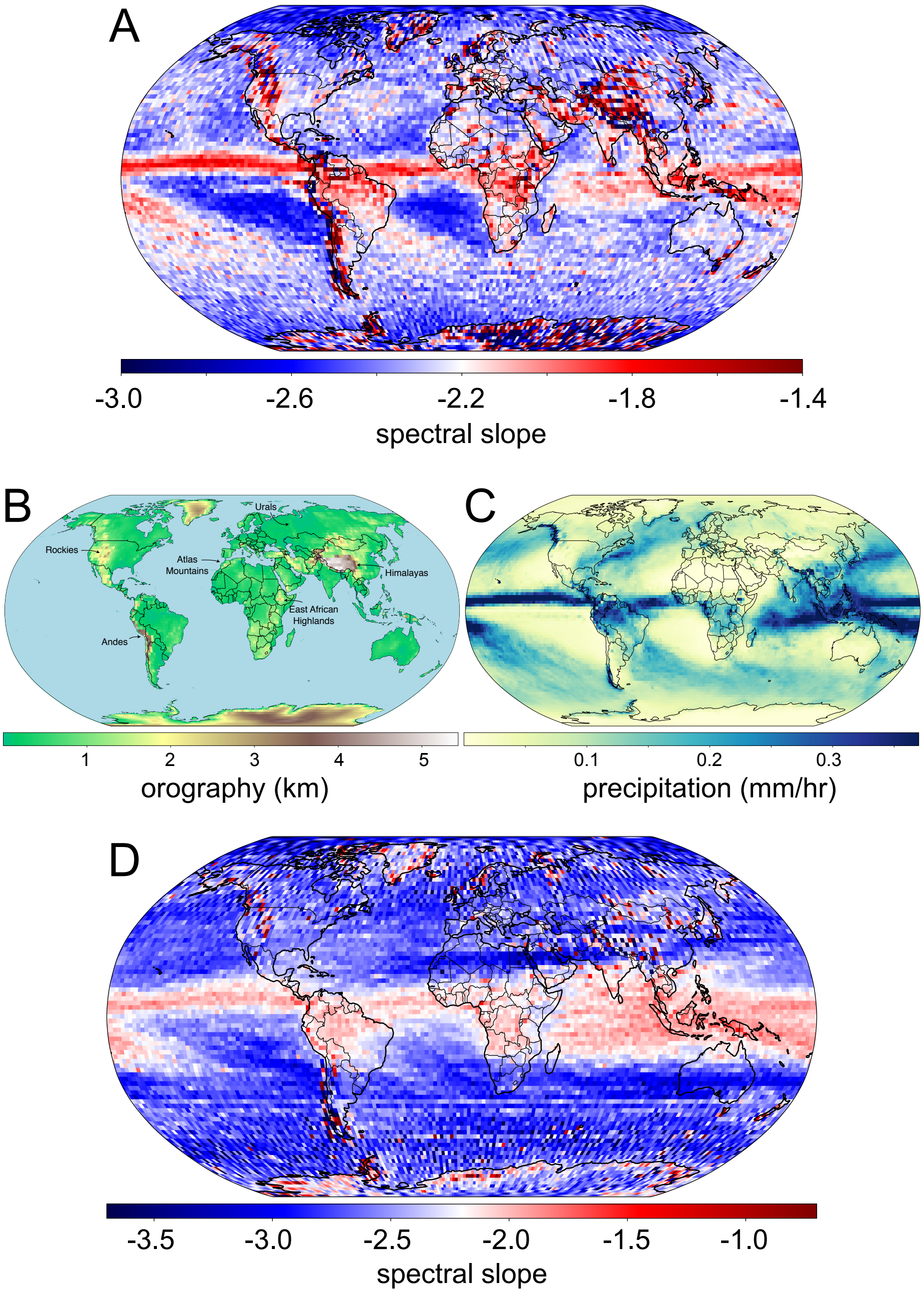

Figure 1: The local slope of the atmospheric kinetic energy spectrum between scales of 100 and 400 km. The 600 hPa, within the troposphere (Fig 1a), and 200 hPa, which straddles the troposphere and stratosphere (Fig 1d), levels are shown. The colour bar is centred at -2.2, close to the global mean slope for illustration. Orography field (Fig 1b) and the 2020 mean precipitation (Fig 1c) for visual comparison. Precipitation is a sign of convective activity. The precipitation field resembles the pattern of shallowing observed at both altitudes. In the troposphere, the orography also has a sizable impact. The combination of orography and precipitation makes a good approximation for the patterns of spectral slope.

Figure 1 visually illustrates the relationship between orography and precipitation and the mesoscale spectral slope. To quantify these relationships, we construct conditional power spectra, utilising the spatial information of the spectra and highlighting the power of our methodology: given a mask/partition over the globe, we can compute the power spectrum averaged only over those points selected by the mask. To measure the impact of convection, we partition the globe based on the quantity of rainfall [see table S1 in Supporting Information], while orography is partitioned based on geographic elevation. The convection masks consider only precipitation over the ocean to remove orographic effects, while the orography masks remove precipitating areas and the poles. This is because the poles contain ice sheets of considerable altitude that are qualitatively different from lower-latitude orography. Figure 2 presents the conditioned spectra and shows a clear shallowing of the power spectra both with increasing precipitation (2a–b) and orographic height (2c–d). The impact of convection is clear at both 600 hPa and 200 hPa (convective precipitation is similar (not shown)), while the orographic effect is significantly weakened at 200 hPa.

We also see a shallowing at 600 hPa associated with the direction of energy flux (Figure 2e), such that points with an upscale (small-scale to large-scale) energy flux exhibit a shallower slope in the mesoscales. This shallowing may be due to the influence of a two-dimensional energy cascade, a possibility that needs further investigation. This effect is not observed in the stratosphere (Figure 2f).

Global Effects of Orography and Convection

Having seen the local effect of orography and convection, it remains to address how these impact the global spectrum. In Figure 3, we compare the global power spectrum with the spectrum computed only over points with no precipitation and sea-level orographic height. At 600 hPa, removing the effects of convection and orography produces a significant steepening of the global spectrum. At 200 hPa, a similar steepening effect is observed for scales smaller than $\sim$ 300 km. This provides evidence that orography and convective activity lead to the shallowing of the mesoscale slope in the troposphere and at higher altitudes.

Mechanisms for spectral shallowing

Three main explanations exist for the shallow spectral slope observed in the atmosphere: i) gravity waves, ii) direct forcing by convection and orography, and iii) turbulent inertial ranges.

i) Gravity Waves

We argue that gravity wave activity dominates the spectral shallowing at 200 hPa. There is a clear resemblance between shallowing at this level and the spatial distribution of gravity wave activity (see the climatology of gravity wave activity at 100 hPa in (Hocke et al., 2016)). While gravity waves can be generated by orography and convection (Hocke et al., 2016), they can be dampened by other features, such as the suppression of gravity waves over the Himalayas caused by the tropical jet. There appear to be steeper slopes at 200 hPa associated with the jet (Figure 1d), particularly when comparing the shallowing seen near the Rockies to that over the Himalayas. This may be due to the suppression of the gravity waves produced by orography, although the interactions between critical layers and topographically induced gravity waves can be complex depending on the details of the atmospheric conditions present (Clark & Peltier, 1984). In addition, convective activity is a strong source of wave activity in the stratosphere (Hocke et al., 2016; Dhaka et al., 2006), consistent with the strong correlation between precipitation and shallow spectral slopes at 200 hPa in Figure 2b.

To further investigate the proposal that gravity waves substantially contribute to the shallowing at 200 hPa, we consider the rotational (horizontally divergence-free) and divergent (irrotational) components of the flow through a Helmholtz decomposition. This strongly correlates with gravity wave activity (Avalos, 2024; Waite, 2020). By applying our coarse-graining methodology to these flow components individually, we find that removing orography and precipitation substantially steepened the divergent flow, while having a minimal effect on the rotational flow [see Supporting Information]. That is, orography and precipitation induce shallowing of the spectrum of the gravity wave field, leading to a shallowing of the full KE spectrum. This indicates that gravity wave effects are likely responsible for the majority of the shallowing associated with orography and precipitation in our maps.

ii) Direct forcing

The second possibility is direct input of energy throughout the mesoscales from topography or convection (Skamarock, 2004). The direct input of energy is distinct from other explanations because it does not suppose that the spectrum is undergoing a cascade independent of the nature of the forcing. This means the particular spectral characteristics of the forcing may influence the observed kinetic energy slope through a kind of imprinting. Both convection and topography exhibit scaling behaviour. For instance, Earth's topography possesses a k^{-2} spectrum (Balmino, 1993) and mesoscale orographic features produce 3D turbulence, thus injecting energy into the flow at their particular scale (Shutts, 2005). Although imprinting is not the dominant explanation globally (when we exclude precipitating and points above sea level from the global spectrum, it undergoes a steepening (Fig 3a) but still exhibits mesoscale shallowing), it may have significant relevance in explaining local shallowing in regions of high orography or precipitation. This possibility deserves further attention. Future investigations may utilise the coarse-graining energy flux to investigate the nature of local energy injection in the mesoscales and or compare local spectral slopes of precipitation and topography to those observed in the kinetic energy.

iii) Turbulent inertial range

The final class of mesoscale slope explanation is inertial range theories. These include the earliest explanations for the mesoscale spectrum (Lilly, 1983). As a class, they share the characteristic that energy is injected at scales larger or smaller than the mesoscales and then undergoes an inertial cascade through it. From observations, it appears that globally, the average flux of energy in the mesoscales is downscale (Cho & Lindborg, 2001), but locally this need not be the case. In Figure 2 e–f, we partition our data based on the local direction of energy transfer through the mesoscales. The relationship between the direction of energy flux and the spectral slope appears weak at 200 hPa (Figure 2f), indicating the two situations produce a comparable spectrum. However, at 600 hPa, local upscale energy flux regions present a shallower spectrum. It is possible that inertial range theories that assumed a global upscale cascade can still be of relevance in explaining this local spectral shallowing in regions of local upscale energy transfer. This possibility of local inertial ranges deserves further attention.

These results demonstrate the striking inhomogeneity and variability of atmospheric spectral slopes. Instead of clean universal power laws, strong regionality and temporal variability is imposed by both orographic and convective effects, including strong localised spectral shallowing (e.g. ITCZ), broad relative steepening in the low-precipitation ‘deserts’ of the south-eastern tropical Atlantic and Pacific basins, and high-variability slopes throughout the globe. Our results not only illustrate these effects, but quantify them, and reveal them to have substantial impacts on spectral characteristics.

Outlook

This work anticipates applying coarse-grain spectral analysis to a whole suite of problems. We will gain new insights into the atmosphere's spectral properties through applying this technique to storms, the quasi-biennial oscillation, El Niño and atmospheric blocking. In addition, the technique promises further insights into spectral variability, including the relationship between spectral slope and geophysical variables such as mean surface level pressure and the magnitude of energy flux. Other further topics of inquiry include predictability, model parametrisation and location-dependent estimates of model effective resolution (Bolgiani et al., 2022). Researchers from adjacent fields could apply the technique to Earth's topography, known to follow a -2 global spectrum (Balmino, 1993), and turbulent flows found in solar, planetary and tokamak physics.

Atmospheric kinetic energy spectra are widely used as a model validation tool (Skamarock, 2004), used to assess both the model's dynamical core (Rauscher et al., 2013) and small-scale approximations (Malardel & Wedi, 2016; Stephan et al., 2022). Our work provides important context for performing such analysis. Only by understanding the origins of the observed spectrum can we use spectral analysis to pinpoint the origins of deficiencies in a model. Furthermore, the Nastrom and Gage spectra (Nastrom et al., 1984), constructed using flight-path data from a set of specific routes, is not representative of the global spectrum and so should not be compared to global model spectra, as is common (Skamarock, 2004).

We hope this report can shift spectral analysis of the atmosphere from a global to a local perspective, allowing us to ask new questions. Future studies may include applying coarse-graining to error growth in global simulations similar to those of Judt, 2018. This would allow a quantification of the error spectrum associated with orography, precipitation or other variables of interest, such as the direction of energy flux. It would also be interesting to analyse the nature of the local mesoscale forcing through coarse-grain energy fluxes to evaluate the relative importance of "direct imprinting" of the spectrum from orography or precipitation against inertial range cascades. In addition, the technique can find many applications in model evaluation, one example being a comparison between the local spectra of ERA5 and IFS to create an effective resolution map of ERA5.

Open research

Code and data are available at Kouhen, 2024.

Acknowledgements

We thank Corwin Wright for an insightful discussion and two anonymous reviewers for their helpful comments.

SK was funded by the Natural Environment Research Council grant number NE/S007474/1. HMC was funded by Natural Environment Research Council grant number NE/P018238/1 and through a Leverhulme Trust Research Leadership Award. HA was funded by US NASA grant 80NSSC18K0772, NSF grant OCE-2123496, US DOE grants DE-SC0014318, DE-SC0020229, DE-SC0019329, NSF grants PHY-2020249, PHY-2206380, and US NNSA grants DE-NA0003856, DE-NA0003914, DE-NA0004134. Computing time was provided by the Texas Advanced Computing Center (TACC) at The University of Texas at Austin, under ACCESS allocation grant EES220052.

Author contributions

SK and HMC conceived the study; BAS and HA wrote the code used to perform the coarse-graining; SK performed the data analysis; SK, BAS, HMC, DPM, and HA wrote the manuscript. BAS, HMC, DPM and HA provided ideas and critical feedback.

Competing interests

The authors declare no competing interests.

References

Aaron Wang, J.-W., & Sardeshmukh, P. D. (2021, may). Inconsistent Global Kinetic Energy Spectra in Reanalyses and Models. *Journal of the Atmospheric Sciences*, *78*(8), 2589–2603. Retrieved from `https://journals.ametsoc.org/view/journals/atsc/aop/JAS-D-20-0294.1/JAS-D-20-0294.1.xml` doi: 10.1175/JAS-D-20-0294.1

Aluie, H. (2019, dec). Convolutions on the sphere: commutation with differential operators. *GEM - International Journal on Geomathematics*, *10*(1), 9. doi: 10.1007/s13137-019-0123-9

Aluie, H., Hecht, M., & Vallis, G. K. (2018). Mapping the Energy Cascade in the North Atlantic Ocean: The Coarse-graining Approach. *Journal of Physical Oceanography*, *48*, 225–244. doi: 10.1175/JPO-D-17-0100.1

Augier, P., & Lindborg, E. (2013). A new formulation of the spectral energy budget of the atmosphere, with application to two high-resolution general circulation models. *Journal of the Atmospheric Sciences*, *70*(7), 2293–2308.

Avalos, Y. (2024). *The role of inertia-gravity waves in the atmospheric energy spectrum: insights from global storm-resolving simulations* (Doctoral dissertation, PhD Thesis). doi: 10.17617/2.3565958

Balmino, G. (1993). The spectra of the topography of the earth, venus and mars. *Geophysical Research Letters*, *20*(11), 1063–1066.

Bolgiani, P., Calvo-Sancho, C., Díaz-Fernández, J., Quitián-Hernández, L., Sastre, M., Santos-Muñoz, D., … Martín, M. (2022). Wind kinetic energy climatology and effective resolution for the ERA5 reanalysis. *Climate Dynamics*, *59*(3-4), 737–752.

Buzzicotti, M., Storer, B. A., Khatri, H., Griffies, S. M., & Aluie, H. (2023, jun). Spatio-Temporal Coarse-Graining Decomposition of the Global Ocean Geostrophic Kinetic Energy. *Journal of Advances in Modeling Earth Systems*, *15*(6). Retrieved from `https://agupubs.onlinelibrary.wiley.com/doi/10.1029/2023MS003693` doi: 10.1029/2023MS003693

Callies, J., Ferrari, R., & Bühler, O. (2014). Transition from geostrophic turbulence to inertia–gravity waves in the atmospheric energy spectrum. *Proceedings of the National Academy of Sciences*, *111*(48), 17033–17038.

Cho, J. Y., & Lindborg, E. (2001). Horizontal velocity structure functions in the upper troposphere and lower stratosphere: 1. observations. *Journal of Geophysical Research: Atmospheres*, *106*(D10), 10223–10232.

Clark, T., & Peltier, W. (1984). Critical level reflection and the resonant growth of nonlinear mountain waves. *Journal of Atmospheric Sciences*, *41*(21), 3122–3134.

Dewan, E. M. (1979). Stratospheric wave spectra resembling turbulence. *Science*, *204*(4395), 832–835.

Dhaka, S., Yamamoto, M., Shibagaki, Y., Hashiguchi, H., Fukao, S., & Chun, H. (2006). Equatorial atmosphere radar observations of short vertical wavelength gravity waves in the upper troposphere and lower stratosphere region induced by localized convection. *Geophysical Research Letters*, *33*. doi: 10.1029/2006GL027026

Gage, K. (1979). Evidence far a k- 5/3 law inertial range in mesoscale two-dimensional turbulence. *Journal of Atmospheric Sciences*, *36*(10), 1950–1954.

Hersbach, H., Bell, B., Berrisford, P., Hirahara, S., Horányi, A., Muñoz-Sabater, J., … others (2020). The ERA5 global reanalysis. *Quarterly Journal of the Royal Meteorological Society*, *146*(730), 1999–2049.

Hocke, K., Lainer, M., Moreira, L., Hagen, J., Fernandez Vidal, S., & Schranz, F. (2016). Atmospheric inertia-gravity waves retrieved from level-2 data of the satellite microwave limb sounder aura/mls. In *Annales geophysicae* (Vol. 34, pp. 781–788).

Judt, F. (2018). Insights into atmospheric predictability through global convection-permitting model simulations. *Journal of the Atmospheric Sciences*, *75*(5), 1477–1497.

Kolmogorov, A. N. (1941). The local structure of turbulence in incompressible viscous fluid for very large reynolds numbers. *Cr Acad. Sci. URSS*, *30*, 301–305.

Kouhen, S. (2024). Spatial spectra of the atmosphere [ComputationalNotebook][Dataset]. Retrieved from `https://doi.org/10.5281/zenodo.11618113` doi: 10.5281/zenodo.11618113

Lilly, D. K. (1983). Stratified turbulence and the mesoscale variability of the atmosphere. *Journal of Atmospheric Sciences*, *40*(3), 749–761.

Lindborg, E. (1999). Can the atmospheric kinetic energy spectrum be explained by two-dimensional turbulence? *Journal of Fluid Mechanics*, *388*, 259–288.

Lindborg, E. (2006). The energy cascade in a strongly stratified fluid. *Journal of Fluid Mechanics*, *550*, 207–242.

Lindborg, E., & Cho, J. Y. (2001). Horizontal velocity structure functions in the upper troposphere and lower stratosphere: 2. theoretical considerations. *Journal of Geophysical Research: Atmospheres*, *106*(D10), 10233–10241.

Malardel, S., & Wedi, N. P. (2016). How does subgrid-scale parametrization influence nonlinear spectral energy fluxes in global nwp models? *Journal of Geophysical Research: Atmospheres*, *121*(10), 5395–5410.

Nastrom, G., Gage, K., & Jasperson, W. (1984). Kinetic energy spectrum of large- and mesoscale atmospheric processes. *Nature*, *310*(5972), 36–38.

Rauscher, S. A., Ringler, T. D., Skamarock, W. C., & Mirin, A. A. (2013). Exploring a global multiresolution modeling approach using aquaplanet simulations. *Journal of Climate*, *26*(8), 2432–2452.

Sadek, M., & Aluie, H. (2018). Extracting the spectrum of a flow by spatial filtering. *Physical Review Fluids*, *3*(12), 124610.

Selz, T., Bierdel, L., & Craig, G. C. (2019). Estimation of the variability of mesoscale energy spectra with three years of cosmo-de analyses. *Journal of the Atmospheric Sciences*, *76*(2), 627–637.

Shutts, G. (2005). A kinetic energy backscatter algorithm for use in ensemble prediction systems. *Quarterly Journal of the Royal Meteorological Society: A journal of the atmospheric sciences, applied meteorology and physical oceanography*, *131*(612), 3079–3102.

Skamarock, W. C. (2004). Evaluating mesoscale nwp models using kinetic energy spectra. *Monthly weather review*, *132*(12), 3019–3032. doi: 10.1175/MWR2830.1

Stephan, C. C., Duras, J., Harris, L., Klocke, D., Putman, W. M., Taylor, M., … Ziemen, F. (2022). Atmospheric energy spectra in global kilometre-scale models. *Tellus A: Dynamic Meteorology and Oceanography*, *74*(1).

Storer, B. A., & Aluie, H. (2023). Flowsieve: A coarse-graining utility for geophysical flows on the sphere. *Journal of Open Source Software*, *8*(84), 4277.

Storer, B. A., Buzzicotti, M., Khatri, H., Griffies, S. M., & Aluie, H. (2022, sep). Global energy spectrum of the general oceanic circulation. *Nature Communi-*

cations, *13*(1), 5314. Retrieved from `https://www.nature.com/articles/s41467-022-33031-3` doi: 10.1038/s41467-022-33031-3

Storer, B. A., Buzzicotti, M., Khatri, H., Griffies, S. M., & Aluie, H. (2023, dec). Global cascade of kinetic energy in the ocean and the atmospheric imprint. *Science Advances*, *9*(51). Retrieved from `https://www.science.org/doi/10.1126/sciadv.adi7420` doi: 10.1126/sciadv.adi7420

Sun, Y. Q., Rotunno, R., & Zhang, F. (2017). Contributions of moist convection and internal gravity waves to building the atmospheric- 5/3 kinetic energy spectra. *Journal of the Atmospheric Sciences*, *74*(1), 185–201.

Tulloch, R., & Smith, K. S. (2009). Quasigeostrophic turbulence with explicit surface dynamics: Application to the atmospheric energy spectrum. *Journal of the atmospheric sciences*, *66*(2), 450–467.

Vallis, G., Shutts, G., & Gray, M. (1997). Balanced mesoscale motion and stratified turbulence forced by convection. *Quarterly Journal of the Royal Meteorological Society*, *123*(542), 1621–1652.

Vallis, G. K. (2017). *Atmospheric and oceanic fluid dynamics.* Cambridge University Press.

Waite, M. L. (2020). Untangling waves and vortices in the atmospheric kinetic energy spectra. *Journal of Fluid Mechanics*, *888*, F1.

Waite, M. L., & Bartello, P. (2006). The transition from geostrophic to stratified turbulence. *Journal of Fluid Mechanics*, *568*, 89–108.

Waite, M. L., & Snyder, C. (2009). The mesoscale kinetic energy spectrum of a baroclinic life cycle. *Journal of the atmospheric sciences*, *66*(4), 883–901.

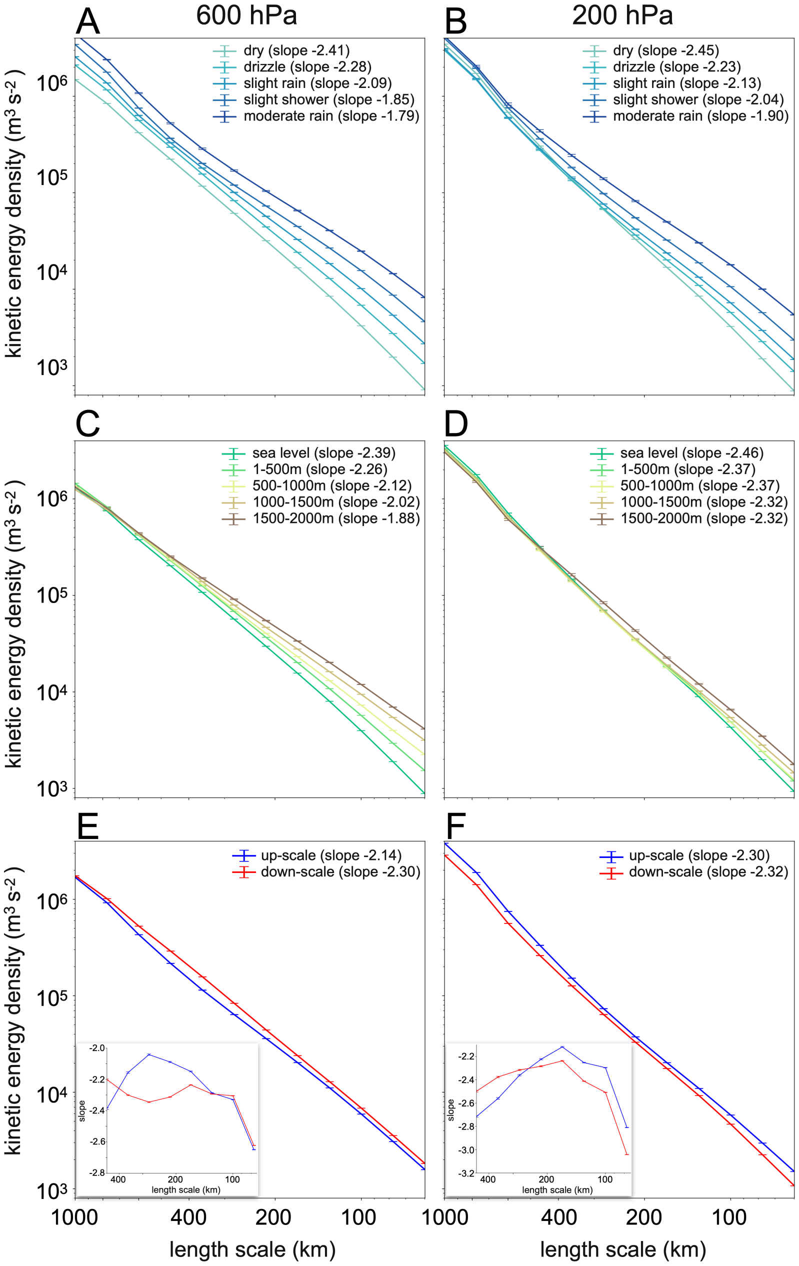

Figure 2: Mesoscale spectra are binned based on their (a–b) level of precipitation and (c–d) orographic height; in (a–b), precipitating points are taken only from over the ocean, and in (c–d) we exclude both precipitating points and the poles from the orography spectra. Precipitation is used as a measure of convective activity. Error bars are obtained through bootstrapping using 1000 sample spectra constructed from 32400 points (equivalent to two globes of data). We exclude heavier rainfall and higher altitude bins due to an insufficient sample size for bootstrapping. The conditioned spectra quantify the clear shallowing effect of precipitation and orographic height in the analysis and the attenuated effect of orography at higher altitudes. In (e–f), spectra are binned based on the local direction of energy flux.Inlaid figures show spectral slope with scale, demonstrating significance. At 600 hPa a shallowing is seen in the mesoscales associated with a local upscale transfer of energy.

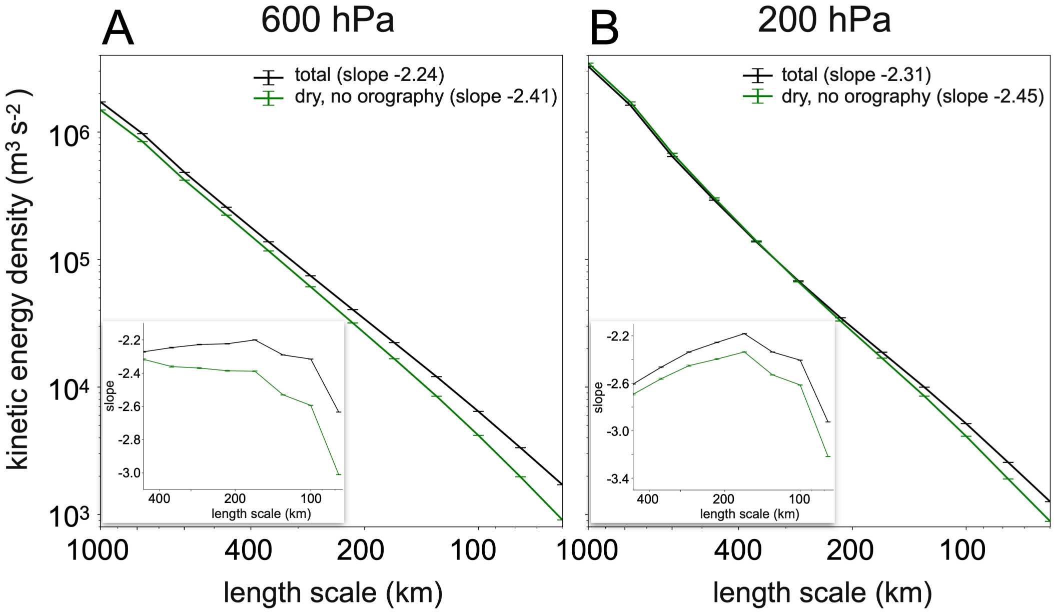

Figure 3: The total global mesoscale spectrum and the global spectrum excluding both land points and precipitating points. Data are shown for 600 hPa (Fig 3a) and 200 hPa (Fig 3b). The total spectrum steepens noticeably when excluding precipitating and land points, indicating the role convection and orography play in shallowing the global spectrum.